Synthesis and Electrochemical Property of Boron-Doped Mesoporous Carbon in Supercapacitor

Da-Wei Wang,[†] Feng Li,[†] Zhi-Gang Chen,[†] Gao Qing Lu,[‡] and Hui-Ming Cheng*,[†]

Shenyang National Laboratory for Materials Science, Institute of Metal Research, Chinese Academy of Sciences, 72 Wenhua Road, Shenyang 110016, P. R. China, and Australian Research Council Centre for Functional Nanomaterials, AIBN, and School of Engineering, The University of Queensland, QLD 4072, Australia

Received June 25, 2008. Revised Manuscript Received September 19, 2008

Mesoporous carbon with homogeneous boron dopant was prepared by co-impregnation and carbonization of sucrose and boric acid confined in mesopores of SBA-15 silica template. Low-level boron doping shows catalytic effect on oxygen chemisorption at edge planes and alters electronic structure of space charge layer of doped mesoporous carbon. These characteristics are responsible for substantial improvement of interfacial capacitance by 1.5−1.6 times higher in boron-doped carbon than that in boron-free carbon with alkaline electrolyte (6 M KOH) and/or acid electrolyte (1 M H_2SO_4). This finding should be very useful for developing new doped carbon electrode materials for supercapacitors.

1. Introduction

In response to the ever increasing demands for clean energy technologies, supercapacitors are considered the most promising energy storage and power output technologies for portable electronics, electric vehicles, and renewable energy systems operated on intermittent sources such as solar and wind. Porous carbons, transition metal oxides, and conducting polymers are fundamental candidates as supercapacitors electrode materials. However, metal oxides and conducting polymers are disturbed by several key drawbacks. For example, metal oxides are either too expensive (RuO_2) or poorly conductive (NiO, MnO_2, etc.); and conducting polymers show short cycling life.[1−3] On the other side, porous carbon materials have been commercially applied in supercapacitor for years, because of their availability with stable physicochemical properties, good conductivity, and low cost.[1−3] Even so, for the emerging applications, fundamental improvements of carbon electrode materials are needed.

Energy storage in carbon-based supercapacitors depends on charge uptake in the carbon/electrolyte interfacial region, which relates to the surface chemical and electronic structure of porous carbons.[1−3] Surface chemical functional groups significantly increase the interfacial capacitance by introducing pseudocapacitance.[4−14] The electronic structure of space charge layer affects electric double layer capacitance.[1,15,16] However, porous carbons as electrode materials are known to suffer from electrode kinetics because of inner-pore ion transport.[17] Porous carbon materials with well-defined oriented mesopore structures are of great importance for energy storage because of the reduced porous tortuosity and facilitated ion transport.[11,13,18−25] Therefore, mesoporous carbon with aligned pore channels combining favorable

* Corresponding author. E-mail: cheng@imr.ac.cn. Fax: 86-24-2390-3126.
[†] Chinese Academy of Sciences.
[‡] The University of Queensland.

(1) Conway, B. E. *Electrochemical Supercapacitors: Scientific Fundamentals and Technological Applications*; Kluwer Academic/Plenum: New York, 1999.
(2) Frackowiak, E.; Beguin, F. *Carbon* **2001**, *39*, 937.
(3) Pandolfo, A. G.; Hollenkamp, A. F. *J. Power Sources* **2006**, *157*, 11.
(4) Hulicova, D.; Yamashita, J.; Soneda, Y.; Hatori, H.; Kodama, M. *Chem. Mater.* **2005**, *17*, 1241.
(5) Ania, C. O.; Khomenko, V.; Raymundo-Pinero, E.; Parra, J. B.; Beguin, F. *Adv. Funct. Mater.* **2007**, *17*, 1828.
(6) Kim, Y. J.; Abe, Y.; Yanaglura, T.; Park, K. C.; Shimizu, M.; Iwazaki, T.; Nakagawa, S.; Endo, M.; Dresselhaus, M. S. *Carbon* **2007**, *45*, 2116.
(7) Kodama, M.; Yamashita, J.; Soneda, Y.; Hatori, H.; Kamegawa, K. *Carbon* **2007**, *45*, 1105.
(8) Hulicova, D.; Kodama, M.; Hatori, H. *Chem. Mater.* **2006**, *18*, 2318.
(9) Li, W. R.; Chen, D. H.; Li, Z.; Shi, Y. F.; Wan, Y.; Huang, J. J.; Yang, J. J.; Zhao, D. Y.; Jiang, Z. Y. *Electrochem. Commun.* **2007**, *9*, 569.
(10) Frackowiak, E.; Lota, G.; Machnikowski, J.; Vix-Guterl, C.; Beguin, F. *Electrochim. Acta* **2006**, *51*, 2209.
(11) Wang, D. W.; Li, F.; Liu, M.; Cheng, H. M. *New Carbon Mater.* **2007**, *22*, 307.
(12) Nian, Y. R.; Teng, H. S. *J. Electrochem. Soc.* **2002**, *149*, A1008.
(13) Li, H. F.; Xi, H. A.; Zhu, S. M.; Wen, Z. Y.; Wang, R. D. *Microporous Mesoporous Mater.* **2006**, *96*, 357.
(14) Raymundo-Pinero, E.; Leroux, F.; Beguin, F. *Adv. Mater.* **2006**, *18*, 1877.
(15) Hahn, M.; Baertschi, M.; Barbieri, O.; Sauter, J. C.; Kotz, R.; Gallay, R. *Electrochem. Solid-State Lett.* **2004**, *7*, A33.
(16) Barbieri, O.; Hahn, M.; Herzog, A.; Kotz, R. *Carbon* **2005**, *43*, 1303.
(17) Wang, D. W.; Li, F.; Liu, M.; Lu, G. Q.; Cheng, H. M. *Angew. Chem., Int. Ed.* **2008**, *47*, 373.
(18) Li, H. Q.; Liu, R. L.; Zhao, D. Y.; Xia, Y. Y. *Carbon* **2007**, *45*, 2628.
(19) Xing, W.; Qiao, S. Z.; Ding, R. G.; Li, F.; Lu, G. Q.; Yan, Z. F.; Cheng, H. M. *Carbon* **2006**, *44*, 216.
(20) Kodama, M.; Yamashita, J.; Soneda, Y.; Hatori, H.; Kamegawa, K.; Moriguchi, I. *Chem. Lett.* **2006**, *35*, 680.
(21) Vix-Guterl, C.; Saadallah, S.; Jurewicz, K.; Frackowiak, E.; Reda, M.; Parmentier, J.; Patarin, J.; Beguin, F. *Mater. Sci. Eng., B* **2004**, *108*, 148.
(22) Liu, H. Y.; Wang, K. P.; Teng, H. S. *Carbon* **2005**, *43*, 559.
(23) Fuertes, A. B.; Lota, G.; Centeno, T. A.; Frackowiak, E. *Electrochim. Acta* **2005**, *50*, 2799.
(24) Jurewicz, K.; Vix-Guterl, C.; Frackowiak, E.; Saadallah, S.; Reda, A.; Parmentier, J.; Patarin, J.; Beguin, F. *J. Phys. Chem. Solids* **2004**, *65*, 287.
(25) Kim, J.; Choi, M.; Ryoo, R. *Bull. Korean Chem. Soc.* **2008**, *29*, 413.

10.1021/cm801729y CCC: $40.75
Published on Web 10/25/2008

electronic structure, active surface chemical environment, and uniform mesopore architecture is expected to show superior ability for supercapacitor technologies.

Because of the recent advancement in the fabrication of ordered mesoporous carbon (OMC), the unique combination of regular mesopore structure, high specific surface area, and tuneable electronic and surface chemical properties has become accessible. For example, chemically oxidized OMC,[11,13,26,27] nitrogen-doped OMC,[20,25,28] and OMC with nanocrystals of metal,[29] oxide,[30,31] or carbide[32] embedded in the framework have been reported. Among these innovative OMC-based materials, the chemically modified ones with oxygen or nitrogen functional groups are greatly promising electrode materials for supercapacitor technologies.[11,13,20,25] Oxygen functional groups contribute pseudofaradaic capacitance by redox reactions between phenol or quinone and acidic or alkaline electrolytes.[2,11,12,14] Nitrogen functional groups are considered to generate pseudocapacitance in the mechanisms of acting as electron donor to attract protons or enhancing charge density of space charge layer,[4,8,33] strengthening oxidation/reduction of quinone,[5] and introducing redox reactions of amine groups.[10] Nonetheless, many other elements (such as boron, sulfur, phosphorus, and halogen) are potential heteroatoms that can improve the performance of OMC for supercapacitor applications. In this work, we attempt to utilize boron-doped mesoporous carbon as superior electrode materials for supercapacitors.

Boron is an unique element that has been explored for decades as substitution in carbon or diamond materials to promote the properties of oxidation resistance, Li-ion insertion, and electrochemical behavior.[34] Boron enters the carbon lattice by substituting for carbon at the trigonal sites[35] and acts as electron acceptor because it has three valence electrons, causing a shift in the Fermi level to the conducting band and hence modifying the electronic structure of boron-doped carbon.[36−38] The change in electronic structure of carbon electrode materials can affect the electric double layer capacitance. Most importantly, low-level boron doping shows catalytic effect on oxygen chemisorption on carbon surface, rendering the introduction of redox reactions related to oxygen functional groups on carbon surface.[34,39,40] Therefore, boron doping is able to modify the electrochemical capacitance of carbon materials, involving electric double layer capacitance and pseudocapacitance.

We report a simple yet efficient method to create boron-doped mesoporous carbon by combining sucrose as carbon precursor, boric acid as boron source and SBA-15 silica host as hard template. The nanoscale mesoporous voids of SBA-15 silica can act as nanoreactors for thermal reactions between boric acid and sucrose-derived carbon. The walls of SBA-15 silica can be removed to form oriented mesopore channels with high mesoporosity. The hard-template route to boron-doped mesoporous carbon can overcome the problems that boron is lost due to chemical reactions of boron with H_2O or CO_2 existing in conventional activation method. The potential use of such fabricated boron-doped mesoporous carbon materials in supercapacitor application was investigated. Remarkably, the boron dopant shows intriguing capability to enhance capacitance of OMC. It was able to achieve an improvement of 1.5−1.6 times in terms of capacitance per surface area with alkaline electrolyte (6 M KOH) and/or acid electrolyte (1 M H_2SO_4).

2. Experimental Section

2.1. Materials Synthesis. OMC was prepared using mesoporous silica (SBA-15) as a hard-template and sucrose as carbon precursor. SBA-15 was infiltrated with sucrose solution (20 wt %) by hard vibrating for 15 min and soaking for another 12 h. For the preparation of boron-doped mesoporous carbon (BMC) with different boron concentration, boric acid was added into the solution with different mass ratio to sucrose (0.075 for BMC-I and 0.15 for BMC-II). Concentrated H_2SO_4 was used as carbonization promoter in a ratio of 0.06 mL per 1 g of sucrose. The mesopores of silica template was thoroughly filled, and this results in the sticky slurry of incorporated silica template with precursors. After infiltration, the samples were heat-treated at 160 °C for 6 h. Thereafter, the sample was carbonized in argon atmosphere at 900 °C for 4 h. The carbonized silica/carbon composite was washed with NaOH dissolved in a deionized water/ethanol (volume ratio 1:1) (0.1 M) solution at 100 °C for 3 h to remove the silica template. Additionally, the boron-doped carbon was further boiled in deionized water at 100 °C for 6 h to extensively dissolve the remaining boron oxide. The obtained carbon was then filtered and rinsed until the pH value was 7, and was finally dried under a vacuum at 100 °C for 12 h.

2.2. Materials Characterization. The X-ray diffraction (XRD) patterns were collected with a Rigaku diffractometer (Cu Kα, λ = 1.5406 Å) at a step scan rate of 0.02° from 1 to 90°. Raman spectra were recorded using micro-Raman spectroscopy (Jobin Yvon LabRam HR800, excited by 632.8 nm He−Ne red laser). TEM (JEOL JEM-2010, 200 kV), EELS mapping (FEI F30, 300 kV), and the samples were dispersed on grid for TEM/EELS observation. Before nitrogen adsorption/desorption (Micromeritics, ASAP 2010 M, 77 K) measurements, the samples were evacuated at 473 K until the manifold pressure was lower than 2 Pa. The atomic concentrations of carbon, oxygen, and boron were determined by X-ray photoelectron spectrometer (ESCALAB 250) with Al Kα radiation (15 kV, 150 W) under a pressure of 4×10^{-8} Pa. The weight ratio of boron was determined precisely through inductively coupled plasma optical emission spectrometry (ICP-OES, Thermo iCAP 6300 ICP-OES).

(26) Bazula, P. A.; Lu, A. H.; Nitz, J. J.; Schuth, F. *Microporous Mesoporous Mater.* **2008**, *108*, 266.
(27) Lazaro, M. J.; Calvillo, L.; Bordeje, E. G.; Moliner, R.; Juan, R.; Ruiz, C. R. *Microporous Mesoporous Mater.* **2007**, *103*, 158.
(28) Xia, Y. D.; Mokaya, R. *Adv. Mater.* **2004**, *16*, 1553.
(29) Choi, W. C.; Woo, S. I.; Jeon, M. K.; Sohn, J. M.; Kim, M. R.; Jeon, H. J. *Adv. Mater.* **2005**, *17*, 446.
(30) Zhu, S. M.; Zhou, H. A.; Hibino, M.; Honma, I.; Ichihara, M. *Adv. Funct. Mater.* **2005**, *15*, 381.
(31) Fan, J.; Wang, T.; Yu, C. Z.; Tu, B.; Jiang, Z. Y.; Zhao, D. Y. *Adv. Mater.* **2004**, *16*, 1432.
(32) Yu, T.; Deng, Y. H.; Wang, L.; Liu, R. L.; Zhang, L. J.; Tu, B.; Zhao, D. Y. *Adv. Mater.* **2007**, *19*, 2301.
(33) Lota, G.; Lota, K.; Frackowiak, E. *Electrochem. Commun.* **2007**, *9*, 1828.
(34) Wu, X. X.; Radovic, L. R. *J. Phys. Chem. A* **2004**, *108*, 9180.
(35) Lowell, C. E. *J. Am. Ceram. Soc.* **1967**, *50*, 142.
(36) Morita, T.; Takami, N. *Electrochim. Acta* **2004**, *49*, 2591.
(37) Shiraishi, S.; Kibe, M.; Yokoyama, T.; Kurihara, H.; Patel, N.; Oya, A.; Kaburagi, Y.; Hishiyama, Y. *Appl. Phys. A: Mater. Sci. Process.* **2006**, *82*, 585.
(38) Vishwakarma, P. N.; Subramanyam, S. V. *J. Appl. Phys.* **2006**, 100.
(39) Radovic, L. R.; Karra, M.; Skokova, K.; Thrower, P. A. *Carbon* **1998**, *36*, 1841.
(40) Zhong, D. H.; Sano, H.; Uchiyama, Y.; Kobayashi, K. *Carbon* **2000**, *38*, 1199.

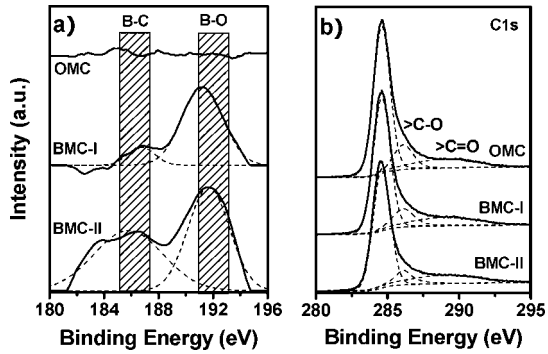

Figure 1. XPS spectra of B1s (a) and C1s (b) signals of ordered mesoporous carbon and boron-doped carbon.

Table 1. Element Distribution and Porosity Parameters Obtained from the XPS Analysis and Nitrogen Sorption Isotherm for the OMC, BMC-I, and BMC-II

sample	initial mass ratio of boric acid/sucrose	C_{XPS} at %	O_{XPS} at %	B_{XPS} at %	$B_{ICP-OES}$ wt %	S_{BET} ($m^2\ g^{-1}$)	V_{total} ($cm^3\ g^{-1}$)
OMC	0	94.1	5.9	0	0	620	0.55
BMC-I	0.075	91.8	8.0	0.2	0.065	660	0.54
BMC-II	0.15	90.2	9.2	0.6	0.16	470	0.49

2.3. Electrochemical Measurements. A mixture of active material, carbon black, and poly(tetrafluoroethylene) (PTFE) at a weight ratio of 90:5:5 was pasted on nickel (6 M KOH electrolyte) or Pt/Rh (1 M H_2SO_4 electrolyte) mesh as working electrode with an area of 1 cm^2. The mass load of active material was 5 mg cm^{-2}. The cyclic voltammogram was collected on Solartron 1287 electrochemical instrument from 2 to 50 mV s^{-1}. The potential range for CV was −0.8 to 0 V vs Hg/HgO in KOH electrolyte and 0 to 0.8 V vs SCE in H_2SO_4 electrolyte with Pt plate as counter electrode. Interfacial capacitance (C_i) was calculated following the equation of $C_i = (\int i dV)/(\nu m V S_{BET})$, where i is the average current density of anodic and cathodic branches, V is the potential, ν is the potential sweep rate, m is the mass of active materials, and S_{BET} is the Brunauer−Emmett−Teller (BET) specific surface area.

3. Results and Discussion

3.1. Chemical Analysis. The surface chemical properties of the ordered mesoporous carbon (OMC) and boron-doped mesoporous carbons (BMC-I/II) were characterized using X-ray photoelectron spectroscopy (XPS). Figure 1a displays the detailed B1s XPS spectra of the samples, which are evident for the existence of boron heteroatoms in the forms of B−C and B−O bonds. The boron doping content is increased as the initial mass ratio of boric acid to sucrose increased, which is evident from ICP-OES analysis (Table 1). Oxygen is commonly present in carbon as a consequence of its incorporation in the dangling bonds when the material is exposed to air. The C1s signals is (Figure 1b) broadened on the high energy side (286−290 eV) are noticed, indicating the presence of carbon atoms singly or doubly coordinated with oxygen atoms (C−O, C═O). By fitting the spectra, three peaks can be identified. A distinct peak is observed at a binding energy of 284.6 eV, characteristic of carbon lattice. Two shoulders are found around 289 and 286 eV, which come from the C═O and C−O groups. It is interesting to see the increase in oxygen as the boron doping is enhanced

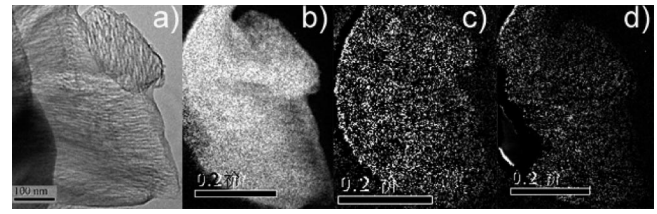

Figure 2. EELS mapping images of BMC-II sample: (a) bright-field image, (b) carbon, (c) oxygen, and (d) boron. The scale bars in b−d are 0.2 μm.

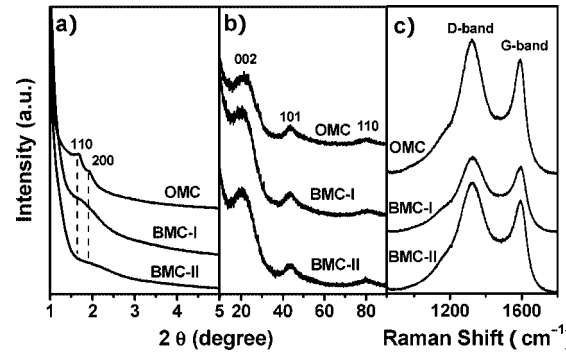

Figure 3. (a) Low- and (b) high-angle X-ray diffraction patterns, and (c) Raman spectra of ordered mesoporous carbon and boron-doped carbon.

(Table 1). Generally, low-concentration boron doping leads to catalytic effect on oxygen chemisorption, as confirmed by experimental and theoretical studies.[34,39,40] Carbon oxidation and oxygen chemisorption are assumed to be electrophilic reactions. The redistribution of π electrons in the presence of substitutional boron weakens C−C bonds and strengthens C−O bonds upon oxygen adsorption.[39] Therefore, it is reasonable to observe higher oxygen concentrations in the boron-doped materials. Figure 2 illustrates the electron energy loss spectroscopy (EELS) mapping images of carbon, oxygen, and boron elements in the BMC-II sample, indicating the homogeneous distribution of boron and oxygen heteroatoms on both the exterior and interior surfaces of the sample. This homogeneous doping is attributed to the liquid-phase co-impregnation of both sucrose and boric acid into the mesopores of SBA-15 silica host, which enables the molecular-level mixing of the sucrose molecules and BO_3^{3-} ions and hence the uniform element distributions in the obtained carbon framework.

3.2. Physical Characterizations. The powder X-ray diffraction (XRD) patterns of the ordered mesoporous carbon and boron-doped carbon are illustrated and compared in panels a and b in Figure 3. The low angle regions of the XRD patterns exhibit peaks that show the mesostructure symmetry of replicated carbons as an indication of long-range structural order (Figure 3a). For the boron-free OMC sample, the XRD patterns show the well resolved (110) and (200) peaks with a hexagonal mesopore arrangement, in good agreement with the SBA-15 silica host. The boron-doped mesoporous carbon samples (BMC-I/II) with different boron concentrations exhibit gradual disappearance of the (100) and (200) peaks, indicating the loss of long-range structural order. The high-angle regions of the XRD patterns illustrate signals that can be assigned to carbon (Figure 3b). Additionally, no other peak is detected showing the absence of boron carbide

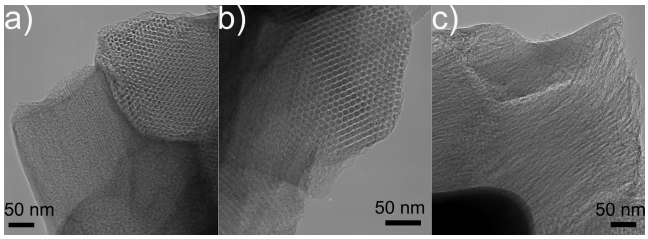

Figure 4. TEM images of mesoporous carbon and boron-doped carbon: (a) image of OMC and (b) image of BMC-I, left particles taken along the [110] direction, right particles taken along the [001] direction, and (c) image of BMC-II taken along the [110] direction.

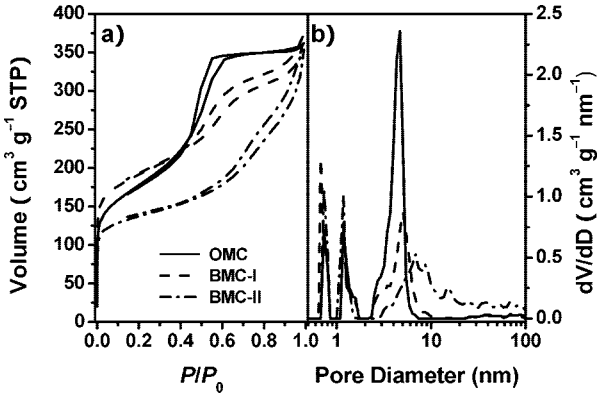

Figure 5. (a) Nitrogen sorption isotherms and (b) pore diameter distribution curves of ordered mesoporous carbon and boron-doped carbon.

or boron oxide, which may be produced during carbonization of sucrose in the presence of boron acid. Raman spectra (Figure 3c) illustrate the D-band and G-band of ordered mesoporous carbon and boron-doped carbon, giving some additional information of the carbon lattice. All samples show the two bands of ca. 1325 cm^{-1} (D-band) and ca. 1592 cm^{-1} (G-band), which are ascribed to the defects/imperfections and hexagonal graphene plane, respectively. The intensity ratio of the D and G bands (I_D/I_G) has a physical meaning for the crystallinity or amorphicity. The I_D/I_G of the BMC-II sample is larger than that of the OMC and BMC-I sample, indicating introduction of defects and imperfections into carbon lattice by boron doping.

The structural arrangements of mesopores in the OMC and BMC samples are studied by transmission electron microscope (TEM) (Figure 4). Well-ordered arrays of carbon nanorods and pore channels are clearly observed for OMC and BMC-I samples. From the TEM image, it is possible to estimate that the carbon nanorod has a diameter of ca. 7 nm with a unit cell size of 18−20 nm, showing a well-defined two-dimensional hexagonal ordered mesostructure. On the other side, although the mesostructure of BMC-II losses the long-range order in (100) plane, it still retains the oriented mesopore alignment along the [001] direction but at the expense of some tortuosity (Figure 4c).

The nitrogen sorption isotherm of OMC shows representative type IV isotherm with a H2 hysteresis loop (Figure 5a). Clear capillary condensation occurs at a relative pressure (P/P_0) of 0.45−0.6, indicating a narrow mesopore diameter distribution with a peak value of 4.6 nm (Figure 5b). The hysteresis loop of BMC-I sample consists of two regions at relative pressures of 0.45−0.66 and 0.66−0.99, showing broadness in the mesopore diameter distribution as confirmed in Figure 5b with a peak value of 4.9 nm and a shoulder in the large pore side. By further enhancing boron doping level, the hysteresis loop of BMC-II sample exhibits a relative pressure range of 0.45−0.99 without the feature of H2 loop, demonstrating the formation of wide mesopore distribution with a peak value of 6.8 nm and a broad shoulder ranging from 10 to 100 nm. The BET specific surface areas of the boron-doped mesoporous carbon are 470−660 $m^2\ g^{-1}$ (Table 1). The BET specific surface area increases initially from 620 to 660 $m^2\ g^{-1}$ with boron doping, implying more micropores, whereas higher boron content results in lowered specific surface area, indicating the loss of micropores.

3.3. Electrochemical Properties. Cyclic voltammetry plots of OMC, BMC-I, and BMC-II samples recorded in 1 M H_2SO_4 electrolyte with a SCE reference electrode are compared in Figure 6a. To establish the comparison, the current density was normalized to interfacial capacitance. The BMC samples show larger interfacial capacitance than that of OMC, which is associated with the boron-incorporated surface chemical structures. The peak interfacial capacitance of OMC (0.3 V versus SCE in the cathodic branch) exhibits an inferior surface reactivity, with a interfacial capacitance of 0.14 F m^{-2}. On the contrary, the boron-doped samples show superior interfacial capacitance, with 0.17 and 0.21 F m^{-2} for BMC-I/II. The interfacial capacitance is composed of pseudofaradaic capacitance and double layer capacitance. In protonic electrolyte, the pseudofaradaic capacitance involves proton exchange between quinone/hydroquinone complexes.[12] The boron doping enhances the concentration of oxygen groups, as analyzed by XPS method. It is thus reasonable to obtain a higher redox capacitance in the boron doped carbons. On the other hand, the double layer capacitance is dependent on the charge density of space charge layer and the density of states (DOS) at the Fermi level, which is tailorable using the heteroatoms doped in carbon lattice.[15,16] Boron atom has three valence electrons, less than that of carbon atom by one electron, and can introduce a hole charge carrier once it replaces a carbon atom in the graphene lattice, which will increase the charge density and DOS, and hence the double layer capacitance.[37]

Considering the proton-free nature of alkaline electrolyte, we further tested the interfacial capacitance of boron-doped carbon in 6 M KOH with a Hg/HgO reference electrode, as shown in Figure 6b. The highest interfacial capacitance at a potential of −0.7 V versus Hg/HgO (cathodic branch) is 0.19, 0.22 and 0.31 F m^{-2} for OMC, BMC-I, and BMC-II. In proton-free KOH, the phenol-/carboxyl-type groups are electrochemically deprotonated, producing pseudofaradaic capacitance.[2] The enhanced total interfacial capacitances of BMC samples in KOH electrolyte are thus also attributed to the improved pseudocapacitance arising from increased oxygen groups and the enhanced double layer capacitance by boron substitution.

Figure 7 demonstrates the relationships between potential sweep rate and gravimetric and interfacial capacitance. It is noted that the gravimetric and interfacial capacitance of boron-doped carbon is higher than the boron-free sample over

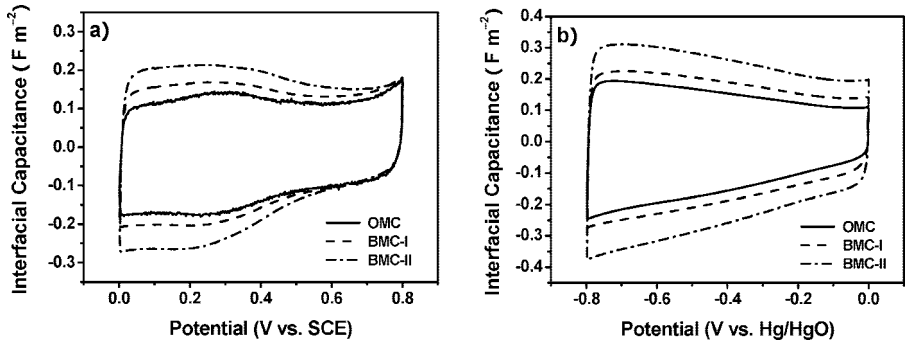

Figure 6. Cyclic voltammetry plots of OMC, BMC-I and BMC-II samples in (a) 1 M H_2SO_4 electrolyte and (b) 6 M KOH electrolyte recorded at 10 mV s^{-1}.

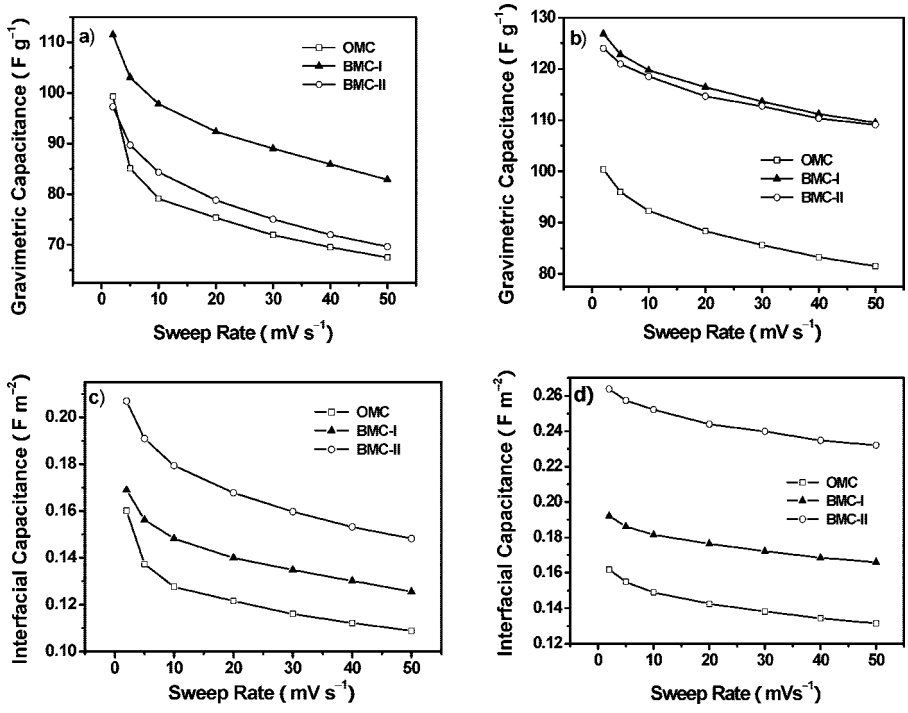

Figure 7. Dependence of calculated gravimetric and interfacial capacitance of OMC, BMC-I, and BMC-II samples on potential sweep rate (from 2 to 50 mV s^{-1}) in (a, c) 1 M H_2SO_4 electrolyte and (b, d) 6 M KOH electrolyte.

all the sweep rates. At low rates, ions can reach both the inner and exterior surfaces of carbon materials, whereas at high rates, only the exterior surface is accessible.[17] The interfacial capacitance enhancement is independent of sweep rate, and this relates to the homogeneous boron doping in both the exterior and inner surfaces. However, the interfacial capacitance of all samples decreases as the sweep rate increases, which is probably due to the calculation method by dividing gravimetric capacitance with BET specific surface area. The ion-accessible surface area, or electrochemical reactive surface area, minimizes as elevating the sweep rate, and in turn results in the reduced gravimetric capacitance.[17] The rate-dependent gravimetric capacitance is the reason why interfacial capacitance reduces as sweep rate increases according to our calculation.

These results suggest that the increased interfacial capacitance of BMC samples in both acidic and alkaline electrolyte originates from (1) the accumulated oxygen groups originated from catalytically enhanced oxygen chemisorption by low-concentration boron dopant, and (2) the increased charge carrier concentration and Fermi level DOS due to the substitutional boron as *p*-dopant. BMC samples are rich in oxygen but with low-level boron doping (<1 at %). The interfacial capacitances of several oxygen-enriched mesoporous carbons prepared using different mesoporous silica templates and carbon precursors are compared in Table 2. It is clear that the boron-doped BMC-II sample in our work shows the highest interfacial capacitance.

It is worth comparing the ability of boron and nitrogen heteroatoms on enhancing the interfacial capacitance of doped carbon at the same oxygen concentration, in order to select the most efficient electrochemically active dopant. In the same electrolyte (1 M H_2SO_4), nitrogen-enriched OMC sample has a higher interfacial capacitance of 0.31 F m^{-2} than that of BMC-II (0.21 F m^{-2}).[20] However, taking into account of the much lower boron concentration (B/C < 0.01) in BMC-II compared to the nitrogen concentration in the nitrogen-enriched carbon (N/C = 0.11),[20] we can expect a much better effect of boron dopant on the enhancing interfacial capacitance at carbon/electrolyte interfacial regions.

In addition, greater enhancement in interfacial capacitance may be achievable by increasing the concentration of boron

Table 2. Comparison of Interfacial Capacitance (C_i, F m^{-2}) of Oxygen-Enriched Mesoporous Carbon Prepared with Different Mesoporous Silica Templates

mesoporous silica template	carbon precursor/carbonization temperature (°C)	modification	C_i 1 M H_2SO_4 (F m^{-2})	C_i 6 M KOH (F m^{-2})	ref
MCM-48	sucrose/900	no	0.096	0.09	21*a*
	propylene/747	no	0.13	0.096	21*a*
	pitch/952	no	0.099	0.12	21*a*
	phenolic resin/900	gasification	0.16	N/A	22*a*
SBA-16	furfuryl alcohol/800	no	0.1	0.11	23*a*
SBA-15	sucrose/900	no	0.11	0.12	24*a*
	propylene/747	no	0.087	0.078	24*a*
	phenolic resin/900	HNO_3 oxidation	N/A	0.24	13
	sucrose/900	HNO_3 oxidation	N/A	0.19	11
	sucrose/900	low-level B-doping	0.21	0.26	BMC-II

[a] C_i not provided in publication. Listed data here were calculated by dividing the given maximum gravimetric capacitance with corresponding BET specific surface area (S_{BET}).

in carbon materials to the maximum value of 2.35 at.%, which is four times of our doping level (maximum 0.6 at.%).[35] Even though, one has to bear in mind that boron substitution in carbon lattice will inhibit oxygen chemisorption above a critical concentration, as observed around 2% by Radovic et al.[39] Therefore, molecular level optimization on the design and synthesis conditions of boron-doped porous carbons or nanostructured carbons is necessary for achieving the highest interfacial capacitance enhancement.

4. Conclusions

We synthesized boron-doped mesoporous carbon using mesoporous silica as hard template, sucrose as carbon precursor, and boric acid as boron *p*-dopant source. This boron-doped mesoporous carbon material possesses the characteristics of aligned mesopores, catalytically rich oxygen functional groups and improved electronic structure in space charge layer. Taking advantage of these characteristics, boron-doped carbon exhibited interfacial capacitance as high as 1.6 times of that with boron-free carbon. Such boron-doped mesoporous carbon can be expected to show maximum capacitance if further optimization of the local boron-doping environment is done.

Acknowledgment. The authors acknowledge financial support from the National Natural Science Foundation of China (50632040).

CM801729Y